



Sub-micron silicon/pyrolyzed carbon@natural graphite self-assembly composite anode material for lithium-ion batteries



Zhoulu Wang^a, Zemin Mao^a, Linfei Lai^a, Masayoshi Okubo^a, Yinghong Song^b, Yingjie Zhou^c, Xiang Liu^{a,*}, Wei Huang^{a,*}

^a Key Laboratory of Flexible Electronics (KLOFE) & Institute of Advanced Materials (IAM), National Jiangsu Synergistic Innovation Center for Advanced Materials (SICAM), Nanjing Tech University (Nanjing Tech), 30 South Puzhu Road, Nanjing 211816, China

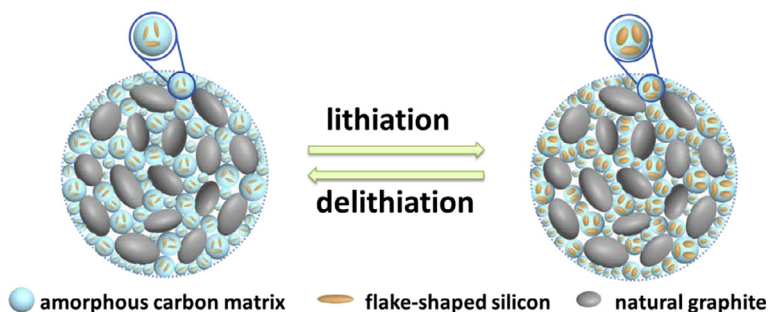
^b Aviation Key Laboratory of Science and Technology on Materials and Application Research for Vibration and Noise Reduction, Beijing Institute of Aeronautical Materials, Beijing 100095, China

^c Department of Materials Physics, School of Physics and Optoelectronic Engineering, Nanjing University of Information Science & Technology, 219 Ningliu Road, Nanjing, Jiangsu 210044, China

HIGHLIGHTS

- The self-assembly of NG and SAN/Si composite microspheres via spray-drying.
- Hierarchical structure with carbon coating and voids buffers the volume change of Si.
- The Si/C@NGs composites deliver high capacity and high first Coulombic efficiency.

GRAPHICAL ABSTRACT



ARTICLE INFO

Article history:

Received 30 September 2016

Received in revised form 27 November 2016

Accepted 15 December 2016

Available online 18 December 2016

Keywords:

Si/C composite

Lithium-ion batteries

Self-assembly

Sub-micron silicon

ABSTRACT

Si/C@NGs composite containing flake-shaped sub-micron sized silicon (Si) enwrapped by pyrolyzed carbon and natural graphite (NG) was successfully prepared by spray-drying-assisted self-assembly method and was systematically studied as an anode material for lithium-ion batteries. The as-prepared Si/C@NGs composite material has a loading amount of sub-micron sized silicon as low as 6.7 wt%. The Si/C@NGs composite has a hierarchical structure with Si/C embedded into natural graphite which further assembles into larger secondary particles of ~20–50 μm . Compared with pure silicon, the as-synthesized Si/C@NGs composite has multi-layer carbon coating as well as voids to alleviate the structural changes of Si during charging/discharging, exhibits an initial efficiency of 82.8% and a capacity retention of 428.1 mA h g^{-1} (1524.0 mA h g^{-1} vs. Si) after 100 cycles at 0.1 A g^{-1} . The remarkable cycling performances, high initial cycle efficiency together with low-cost manufacturing process make Si/C@NGs composite appealing for commercial applications.

© 2016 Elsevier B.V. All rights reserved.

1. Introduction

In recent years, lithium-ion batteries have become important green power sources for portable electronics and electric vehicles [1,2]. Silicon (Si) electrode exhibits an extraordinarily large theoretical capacity of 4200 mA h g^{-1} which is over 10 times greater

* Corresponding authors.

E-mail addresses: iamxliu@njtech.edu.cn (X. Liu), iamwhuang@njtech.edu.cn (W. Huang).

than that of graphite [3]. However, the practical applications of Si anode have been impeded, mainly due to its huge volume change ($\sim 300\%$) during lithium insertion/extraction, resulting in loss of electrical continuity and progressive pulverization, and fast capacity fading [4,5]. Size reduction of Si to micro/nanometer range and the introduction of the electronic conductors can tackle the aforementioned problems to a certain extent [6,7]. However, the high surface area and low tap density are likely to result in other issues, such as high cost, low first cycle efficiency, low volumetric energy density and agglomeration of nano silicon during charge/discharge [8]. Therefore, graphite is still the most commonly used negative electrodes due to its low cost and stable cycle performance until now [9]. Yet, the relatively lower intrinsic capacity (372 mA h g^{-1}) of graphite is below the expectation with the emergence of high energy electric vehicles and stationary utility grids [10]. But, it should be noted that the main stream commercial cathode materials have much lower discharge capacities of $140\text{--}170 \text{ mA h g}^{-1}$ (e.g., LiCoO_2 or LiFePO_4) [11,12], compared with that of graphite anode. Therefore, the requirement for significantly high capacity anode is trivial, considering the other issues of Si based anode, such as low first cycle efficiency, capacity loss, and low volumetric energy [13]. Si/graphite composite materials with low weight ratio of Si that yield reasonable capacity improvement, high first cycle efficiency and long cycle life are highly desirable.

Integration of commercially available Si nanoparticles with various carbon matrix is reported to deliver a high capacity. Various Si/carbon composite materials and preparation methods have been developed to avoid the agglomeration issue of nano silicon during cycling, such as depositing Si onto a graphite surface [14], preparing an interconnected porous Si/C nanocomposite particles [15], embedding ultrafine Si materials into continuous film structures [16], utilizing Si-based nanowires [17], and constructing three-dimensional nanoporous Si spheres [18]. Among all the reported Si/C composites, a uniform distribution of nano silicon within the carbon matrix is considered to be of significant importance to prevent Si agglomeration during cycling and accommodate isotropic volume expansion. For example, Si/C with carbonized styrene-acrylonitrile copolymer coating [19], $\text{Si@SiO}_x/\text{C}$ with glucose coating followed by hydrothermal treatment [20], Si@C/GF with Si nanoparticles in-situ grown on graphene framework [21], and Si@C/RGO composite with Si embedded in graphene oxide network [22]. The Si/C has been proven to be an much more effective design to improve the performance of Si nanoparticles, for which the carbon coating acts as a buffer place for volume change of Si during the cycling and serves as an electrical conducting pathway [23]. It is noteworthy that, most of the reported Si/C work use Si nanoparticles with size down to tens of nanometer. Unfortunately, nano Si possesses a low tap density, high surface area and undesirable side reaction due to high surface area in addition to high material cost [24]. Micron-sized or sub-micron size Si with low surface area as well as low price is very promising for large scale applications if it has long cycling life. However, the capacity of micron-sized or sub-micron size Si composite is lower than that of nano Si composite. For example, micron-sized Si particles/N-doped graphene composite has a specific capacity of 510 mA h g^{-1} [24], much lower than that of nano Si and carbon composite ($>1000 \text{ mA h g}^{-1}$) [25].

In an effort to develop Si anode that could be produced in a quality comparable to the industrial standard, and also exhibit good electrochemical performance in terms of good cycle life, improved first cycle efficiency, to match with the standard cathode. In this work, we employed self-prepared ball-milled sub-micron sized Si as precursor. The styrene-acrylonitrile copolymer (SAN) was used as the matrix for Si (SAN/Si) to form primary carbon coating, with graphite as main backbone to provide better mechanical properties. The Si/C@NGs composite with hierarchical

structure was produced by the granulation of nature graphite (NG) particles and SAN/Si composite microspheres via spray-drying, and followed by pyrolysis, as illustrated in Scheme 1 and Scheme 2.

In the electrode structural viewpoint, we adopted sub-micron Si plates with two times of amorphous carbon coating, which further ensures the expansion of Si through voids space inside the coating, while maintaining its electrical conductivity and continuity as well. Recently, SAN-coated anode materials have been demonstrated to have high electrochemical stability and good mechanical properties [26]. Here, the SAN was applied as matrix for Si nanoplates and formed the first carbon coating by dispersion polymerization, and the second carbon coating with numerous voids was generated by the spray-drying process. The electrochemical performance of Si/C@NGs was systematically evaluated, and an initial efficiency of 82.8% with capacity retention of $428.1 \text{ mA h g}^{-1}$ ($1524.0 \text{ mA h g}^{-1}$ vs. Si) after 100 cycles at 0.1 mA g^{-1} was achieved. In addition, it is also found that sub-micron sized silicon ($<10 \text{ wt}\%$) can bring a capacity improvement of 30.4% without significant reduction of the first cycle efficiency when Si/C@NGs used for Li-ion anode.

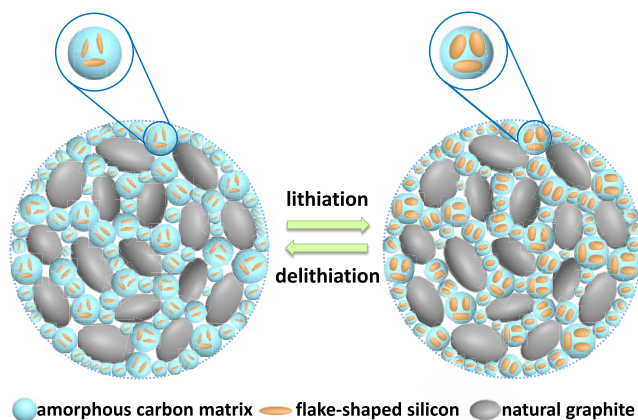
2. Experimental

2.1. Materials

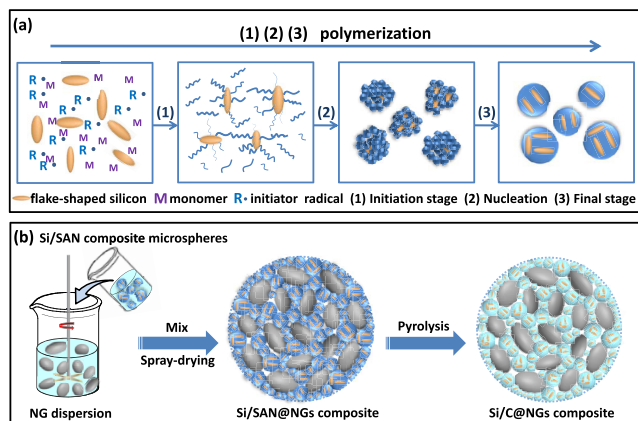
Styrene (St; 99%; Aldrich) and acrylonitrile (AN; 99%, Aldrich) were distilled under reduced pressure to remove inhibitors and held at 0°C before use. Benzoyl peroxide (BPO; 75%, Aldrich), ethanol (99.7%, Aldrich), stearic acid (SA; 9%, Aldrich), 3-(trimethoxysilyl)propyl methacrylate (TMPTS; 97%, Aldrich), polyvinylpyrrolidone (PVPK29-32, $M_r = 58,000$, Aldrich) and carboxymethyl cellulose sodium salt (CMC; dynamic viscosity = $800\text{--}1200 \text{ mPa}\cdot\text{s}$, Aldrich) were used without further purification. Commercial micrometric silicon powder (99.9%, particle size $1\text{--}5 \mu\text{m}$, AlfaAesar) and NG particles (Ao Yu Graphite Group) were purchased.

2.2. Preparation of irregularly flake-shaped sub-micron Si dispersion

The raw silicon powders were dispersed in ethanol at a mass ratio of 1:9, and then the mixture was transferred into a 1 L hardened steel vial with zirconia balls (0.08 mm) at a ball-to-powder ratio of 3:1. Lastly, the mixture was grinded at 3800 rpm for 5 h



Scheme 1. Schematic illustration for the design of hierarchically structured Si/C@NGs composite with Si embedded in between natural graphite and encapsulated with amorphous carbon shell.



Scheme 2. The synthetic mechanism of Si/SAN composite microspheres (a) and the synthesis of Si/C@NGs microspheres by spray-drying assisted self-assembly method (b).

by a nano ball grinder (Pulverisette 5, Fritsch). As the result, the irregularly flake-shaped sub-micron Si particles in the diameter range of 28–342 nm were obtained.

2.3. Hydrophobic treatment of sub-micron Si particles

The surface of flake-shaped sub-micron Si particles was hydrophobicated with SA. 100 g Si dispersion (10 wt% Si) and 0.1 g SA were put into a 250 mL round-bottomed flask equipped with a mechanical stirrer and then stirred for 24 h. The control experiment was performed using Si particles modified with TMPTS. 100 g Si dispersion (10 wt% Si) and 0.5 g TMPTS were put into a 250 mL round-bottomed flask equipped with a reflux condenser and then stirred for 24 h.

2.4. Polymerization procedure of SAN/Si composite microspheres

PVP was dissolved in ethanol at 70 °C for 30 min in a 500 mL four-neck round-bottomed flask equipped with a thermometer, a mechanical stirrer, a reflux condenser, and a nitrogen gas inlet and outlet. Then Si (modified with SA) dispersion was poured into the flask. BPO was dissolved in the mixed monomer (St and AN), then the solution was added into the flask. The flask was immersed into a 70 °C water bath for 7 h under nitrogen protection and the stirring speed was fixed at 210 rpm. The resulted SAN/Si composite microspheres synthesized at various conditions are shown in Table S1, and named as Si-6.5/SAN, Si-10.5/SAN, Si-14.5/SAN and Si-18.5/SAN composite microspheres with different Si contents.

2.5. Synthesis of Si/C@NGs self-assembly composite

NG, CMC solution and deionized water were mixed into a beaker and stirred for 30 min under 3000 rpm. Then Si-18.5/SAN composite microspheres were added into the beaker and stirred for 30 min under 500 rpm. The weight ratio between NG particles, Si-18.5/SAN composite microspheres and CMC was set to 60:40:0.2 and the solid content of the resulting dispersion was 24%. Subsequently, the dispersion was spray-dried to form the self-assembled Si/SAN@NGs composite under the following conditions: the inlet temperature of the spray dryer was 280 °C and the outlet temperature was 120 °C; the rotation speed of the centrifugal atomizer was 35,000 rpm; the injection speed was 10 mL min⁻¹. The Si/SAN@NGs composite was pyrolyzed in three steps under argon atmosphere. Firstly, the Si/SAN@NGs composite

was heated to 375 °C with a heating rate of 2 °C min⁻¹ and kept for 2 h. Secondly, the temperature was increased to 480 °C at 1 °C min⁻¹ and maintained for 3 h. Thirdly, the material was heated up to 900 °C at 2 °C min⁻¹ and kept for 2 h. Above all, the Si/C@NGs self-assembly composite (containing 6.7 wt% Si) was prepared.

2.6. Characterization

To estimate the hydrophobicity of the sub-micron Si particles, the Si modified with TMPTS and the Si modified with SA, the contact angle measurements were performed at room temperature using goniometer (JC2000A, Shanghai Zhongchen Company Limited). Static contact angle of the samples was procured from droplet of deionized water dropped onto the surface of a glass slide. The recorded final value is the average of three measurements of different parts with the same sample.

The surface morphologies of SAN particles, Si/SAN composite microspheres, Si/SAN@NGs and Si/C@NGs composite were observed with a scanning electron microscopy (SEM, JSM6360LV, JEOL) equipped with energy dispersive spectroscopy (EDS, 2000XMS60, GENESIS) attachment at accelerating voltage of 20 kV and Si/C@NGs composite was cut by ion milling system (E-3500, Hitachi). The structure of Si/C@NGs composite was investigated with a transmission electron microscope (TEM, JEM-2100F, JEOL).

The size distribution of sub-micron Si particles was determined by Laser Particle Size Analyzer (MS2000, Malvern).

The compositions on the surface of Si/SAN composite microspheres were characterized by X-ray photoelectron spectroscopy (XPS, PHI 5000 Versa Probe, UIVAC-PHI) experiment.

The thermal properties of pure SAN particles and Si/SAN composite microspheres were studied by the thermogravimetric analyses (TGA, NETZSCH STA 409PC) under N₂ atmosphere from room temperature to 900 °C at a heating rate of 10 °C min⁻¹.

Specific surface areas of the samples were obtained by N₂ adsorption/desorption isotherms using multipoint BET (BELSORP-MINI, Ankersmid).

Raman measurements of NG, sub-micron Si particles and Si/C@NGs composite were performed by micro Raman spectroscopies (Lab RAM HR800, Horiba) at a 514.4 nm excitation wavelength.

The crystal structures of NG, sub-micron Si particles and Si/C@NGs composite were determined by X-ray diffraction (XRD, RINT2000, Rigaku) with Cu K α radiation at 40 kV and 300 mA, 2 θ -step from 10° to 90° at a scan rate of 0.2° s⁻¹.

The working electrodes were made from the homogeneous mixture of 80 wt% active materials (Si/C@NGs composite), 10 wt % Super P and 10 wt% binder (polyvinylidene fluoride) in N-methyl-2-pyrrolidone solvent. The electrodes were coated onto copper foil and dried at 80 °C in vacuum oven for 12 h, and then were cut into circular electrode plate where the mass loading of active materials was approximately 4.63 mg per electrode. Button cells (CR2430) were assembled with the electrolyte (1 M LiPF₆ was in a mixture of ethylene carbonate, diethyl carbonate and methyl carbonate at 1:1:1 by volume), the separator (Celgard-2400) and the reference electrode metallic (lithium foil). Cyclic voltammetry (CV) was measured through an electrochemical system (Model 1470E, Solartron) at a scan rate of 0.05 mV s⁻¹. The discharge and charge performances were investigated by a multi-channel battery testing system (BT2000, Arbin) in a voltage range of 0.01 to 1.5 V vs. Li/Li⁺. The corresponding electrochemical impedance spectra (EIS) were tested by Autolab electrochemical workstation (PGSTAT302N, Metrohm Autolab) with the frequency range of 100 kHz to 0.01 Hz.

3. Results and discussion

3.1. Surface modification of sub-micron Si particles

The surface chemical property of Si is of significant importance to achieve uniform coating of SAN polymer for carbonization. The TMPTS and SA are used as agents for surface treatment of Si, and the water contact angle (θ) is applied to evaluate the hydrophobicity of sample surface. The water contact angle of the surface of Si, the Si modified with TMPTS (TMPTS/Si) and the Si modified with SA (SA/Si) is shown in Table 1, respectively. The surfaces of Si and TMPTS/Si have contact angles of 30.02° and 36.65° with water, which are smaller than 90° indicating both are hydrophilic, while SA/Si has a contact angle of 118.79° with water, representing a hydrophobic surface. The dispersion polymerization of St and AN was carried out in the presence of the above-mentioned three types of sub-micron silicon particles, respectively. Compared with Si and TMPTS/Si, the SA/Si can form a uniform dispersion polymerization without precipitation after days of storage. The SEM images are shown in Fig. 1. It can be seen that the Si/SAN composite microspheres prepared from Si (Fig. 1a) and TMPTS/Si (Fig. 1b) present obvious particle aggregation, while the composites prepared from SA/Si (Fig. 1c) have spherical morphology with better uniformity. Therefore, the SA/Si with high hydrophobicity has beneficial effect on the polymerization stability. Therefore, the SA/Si is used as precursor to prepare Si/SAN composite.

3.2. Structural characterization of SAN particles and Si/SAN composite microspheres

Fig. 2a–f show the SEM images of sub-micron Si particles, pure SAN particles (without Si), Si-6.5/SAN, Si-10.5/SAN, Si-14.5/SAN and Si-18.5/SAN composite microspheres, respectively. It can be seen from Fig. 2a that the Si particles have irregularly flake-like structure, with particle sizes ranging from 28 to 342 nm (size distribution is shown in Fig. S1 and XPS high-resolution spectra of Si 2p in pure Si are shown in Fig. S4). SAN particles and Si/SAN composite microspheres with different Si ratios show spherical shape with a diameter between 281 nm and 2.3 μm . In addition, the surfaces of Si/SAN composite microspheres are relatively smooth and without noticeable uncoated Si particles. The EDS data of Si/SAN composite microspheres with different weight ratios of Si are shown in Table 2. The results indicate the Si content of Si/SAN is in good agreements with the amount of Si added in the recipes shown in Table S1. The surface analysis (C, N and Si) of Si-6.5/SAN to Si-18.5/SAN composite microspheres are listed in Table 3. The XPS measurement is surface analysis method with detection sensitivity above 10 nm, and the low silicon contents on the surface of Si-6.5/SAN to Si-18.5/SAN composite microspheres further prove the full encapsulation of Si in SAN matrix.

Fig. 3 shows TGA of pure SAN particles and Si/SAN composite microspheres with different Si contents measured in nitrogen atmosphere. The significant weight loss of SAN particles starts from 360°C and the initial decomposition temperature of Si/SAN

microspheres is about 375°C . In addition, all the Si/SAN composite microspheres degrade from around 375°C to around 480°C , and the maximum weight loss rate is at about 431°C . The weight loss at 900°C is 96.4% for pure SAN particles, and decreases from 90.2% to 80.6% with increasing of Si content of Si/SAN composite microspheres. The TGA results agree well with a different feeding ratio of Si shown in Table S1.


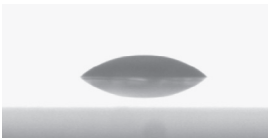

3.3. Structural characterization of Si/C@NGs self-assembly composite

Fig. 4 shows the XRD patterns of NG, Si particles and Si/G@NG composite. For natural graphite, two forms of crystal structure exist, i.e., hexagonal (2H) and rhombohedral (3R) to Graphite (JCPDS No. 65-6212) and Graphite-3R (JCPDS No. 26-1079), the strongest intensity of the peak at $2\theta = 26.54^\circ$ of NG is due to the lamellar structure in graphite [9]. The Si particles have a cubic structure with space group of Fd-3m (JCPDS No. 65-1060), the diffraction peaks at 2θ angle of 28.4° , 47.3° , 56.1° , 69.14° , 76.39° and 88.05° can be readily assigned to diffraction of (111), (220), (311), (400), (311) and (422) faces of silicon. Compared with pure NG and Si, the shape and position of the diffraction peaks remain the same for Si/C@NGs, manifesting that dispersion polymerization, spray-drying and pyrolysis processes do not alter the crystalline structure of Si and NG. The weak intensity of the silicon diffraction peaks can be explicated through the low content of Si (just 6.7 wt%) in Si/C@NGs composite. A broad peak at 23° in Si/C@NGs composite can be attributed to the amorphous carbon that formed during the pyrolysis of SAN.

The Raman spectra of NG, Si particles Si/C@NGs composite are shown in Fig. 5. For Si/C@NGs composite, there is blue shift for the peaks of Si located at 510 , 295 and 943 cm^{-1} , in comparison with those of Si particles (500 , 282 and 910 cm^{-1}). This phenomenon may be due to the phonon confinement effect or a masking effect of amorphous carbon coating on Si particles [27]. The characteristic D band and G band for Si/C@NGs composite are 1344 and 1592 cm^{-1} , respectively, which are related to carbon and graphitic crystallites of carbon materials. The ratio of D band and G band (ID/IG) intensity represents to the graphitization degree, where a lower ratio value signifies a higher graphitization degree [28]. Compared with NG (ID/IG = 0.21), the Si/C@NGs composite has higher ID/IG ratio of 1.03, indicating an increased disorder of the carbon in Si/C@NGs composite due to the presence of amorphous carbon produced from SAN.

The microscopic features of NG, Si/SAN@NGs, and Si/C@NGs composite were characterized by SEM and TEM. Fig. 6a shows the SEM image of NG particles. The average particle size of the NG is about $10\text{ }\mu\text{m}$ and the graphite is irregular ellipsoid with a relatively dense and smooth surface. As seen from Fig. 6b, Si/SAN@NGs composite prepared by spray drying is self-assembled to a spherical structure with a particle size of $15\text{--}50\text{ }\mu\text{m}$. The magnified surface image of Si/C@NGs composite are shown in Fig. 6b. TGA curves of Si, NG and Si/C@NGs under air atmosphere are shown in Fig. S2, and Si/C@NGs composite material just has 6.7 wt% Si particles. Furthermore, some individual

Table 1
The contact angles of Si (a), TMPTS/Si (b), SA/Si (c) with water, respectively.

Sample	(a) Si	(b) TMPTS/Si	(c) SA/Si
Photo			
Water contact angle (θ)/ $^\circ$	30.02	36.65	118.79

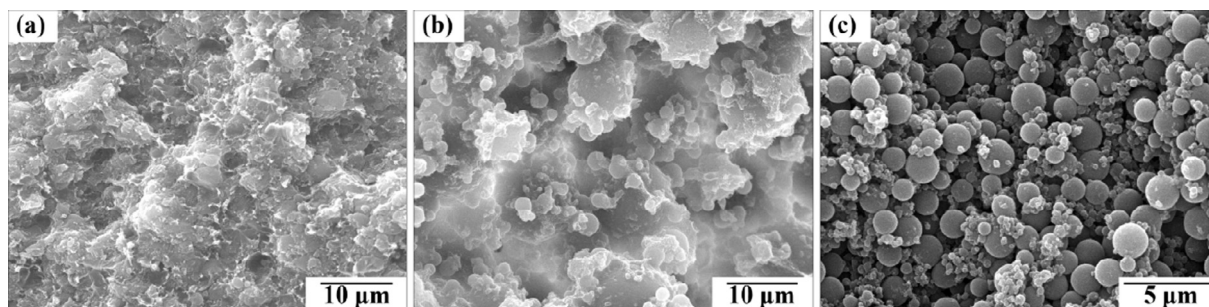


Fig. 1. SEM images of composite microspheres prepared from Si (a), TMPTS/Si (b) and SA/Si (c) with the same Si content, respectively.

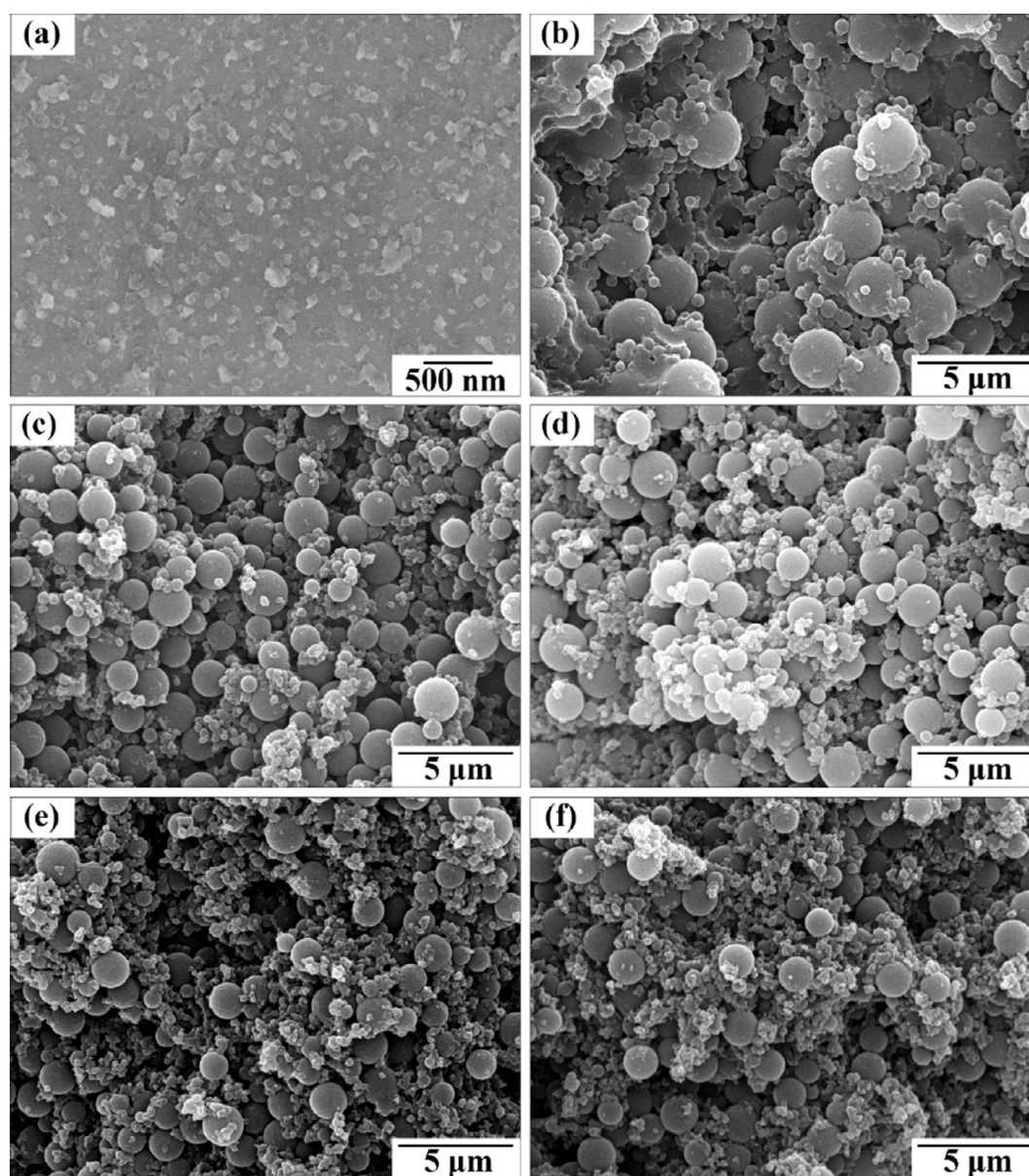


Fig. 2. SEM images of sub-micron Si particles (a), SAN particles (b), Si-6.5/SAN (c), Si-10.5/SAN (d), Si-14.5/SAN (e) and Si-18.5/SAN (f), respectively.

Si/C@NGs composite were cut and then characterized by cross-sectional field-emission SEM and energy dispersive spectroscopy mapping analysis to identify the micro-structure of their interior, and the results are shown in Fig. 6d and e. The results indicate that

the pyrolyzed carbon-coated Si sits in the voids between NG particles thus forms the self-assembly composite. There is a highly porous structure in the interior of the self-assembled Si/C@NGs composite. Obviously, Si particles are in an amorphous carbon

Table 2

The average compositions of Si/SAN composite microspheres with different Si contents analyzed by EDS.

Sample	C/%	Si/%
Si-6.5/SAN	94.08	5.92
Si-10.5/SAN	91.11	8.89
Si-14.5/SAN	88.46	11.54
Si-18.5/SAN	85.13	14.87

Table 3

The compositions on the surface of Si/SAN composite microspheres with different Si contents analyzed by XPS.

Sample	C/%	N/%	Si/%
Si-6.5/SAN	87.44	9.25	3.31
Si-10.5/SAN	87.42	9.88	2.70
Si-14.5/SAN	88.02	8.59	3.39
Si-18.5/SAN	86.72	10.07	3.22

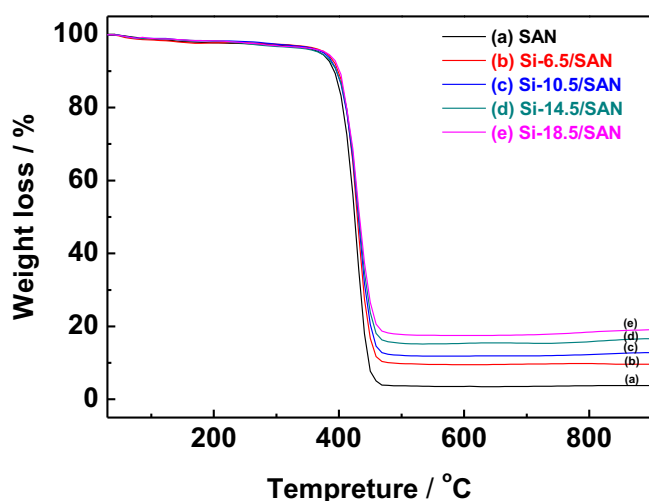


Fig. 3. TGA curves of SAN and Si/SAN composite microspheres with different Si contents under nitrogen atmosphere.

matrix that was derived from the pyrolysis of SAN. The TEM and HRTEM images of Si/C@NGs composite (in Fig. 7) further confirm the embedding of Si particles in an amorphous carbon matrix. The amorphous carbon matrix provide a buffer to adapt for the volume change of Si during discharge/charge process, and prevent the Si particles from agglomeration, consequently stabilizing the structure of the Si and improving the cycling performance. As shown in Table S2, the BET surface areas of Si, NG and Si/C@NGs are 167, 7 and 9 m² g⁻¹, respectively. And the N₂ adsorption-desorption isotherms are shown in Fig. S3 to support the BET results. The lower BET surface area of Si/C@NGs is a prerequisite for high initial Coulombic efficiency and higher volumetric energy density for practical applications.

3.4. Electrochemical properties

The as-prepared Si/C@NGs self-assembly composite was used as an anode material for lithium-ion batteries. Fig. 8 shows the CVs of Si/C@NGs composite anode in the voltage range of 1.5–0.001 V (vs. Li/Li⁺) at 0.05 mV s⁻¹ in the first and second cycle. For the first reduction process, a broad peak around 0.88 V is found, which can be ascribed to the formation of solid-electrolyte interface (SEI) layer on the surface of electrode from the reduction of electrolyte decomposition [29]. The above peak disappears at the

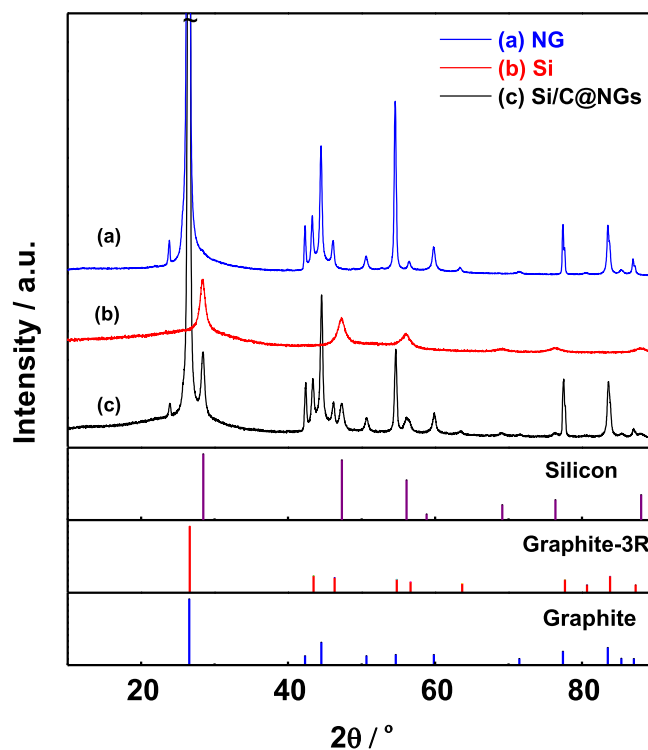


Fig. 4. XRD patterns of NG, Si particles and Si/C@NGs composite.

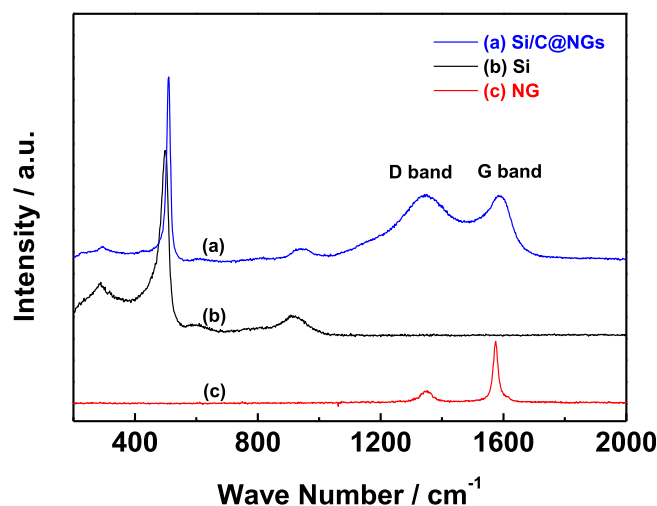


Fig. 5. Typical Raman spectra of Si/C@NGs composite, NG and Si particles.

second cycle, indicating the SEI film is stable during the first lithium insertion and extraction process [30]. In the first and second cycles, there are several cathodic peaks between 0 to 0.2 V and the anodic peaks at a range of 0.13–0.55 V which can be attributed to the lithium-ion insertion and extraction reactions with NG and Si, corresponding to the equation of $x\text{Li} + y\text{Si} \rightleftharpoons \text{Li}_x\text{Si}_y$ and $x\text{Li} + 6\text{C} \rightleftharpoons \text{Li}_x\text{C}_6$. In the second oxidation process of Si/C@NGs composite anode, there were three expected oxidation peaks about delithiation of Li_xC_6 during 0.14–0.25 V, meanwhile, a small broad peak appears around 0.5 V which is related to delithiation of Li_xSi_y . The above results are consistent with characteristics of natural graphite and silicon materials reported earlier [31].

The discharge-charge curves of Si/C@NGs composite electrode between 0.01 and 1.5 V are shown in Fig. 9 in the 1st, 2nd,

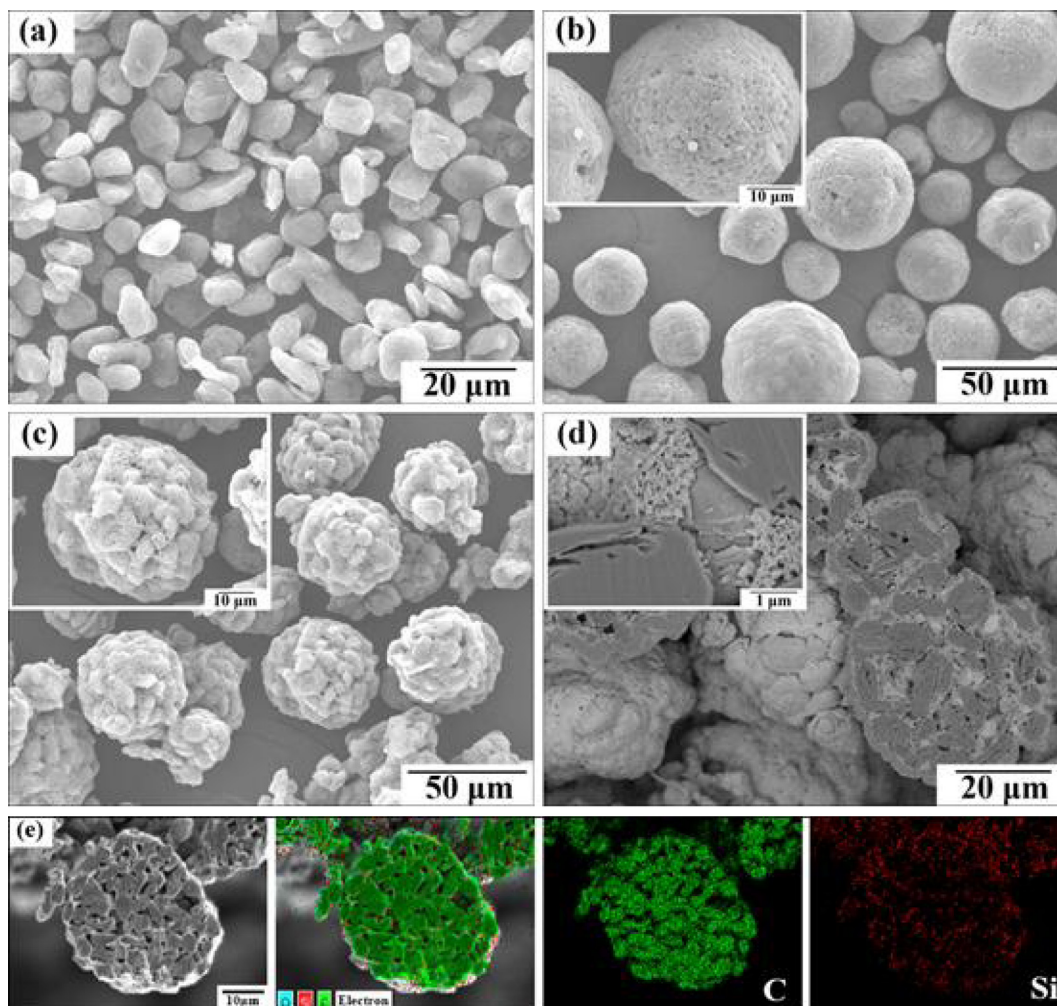


Fig. 6. SEM image of NG particles (a), Si/SAN@NGs composite (b), Si/C@NGs composite after carbonization (c) and cross profile of Si/C@NGs composite (d), STEM images of Si/C@NGs composite for elemental mapping by energy-dispersive spectroscopy (e), respectively.

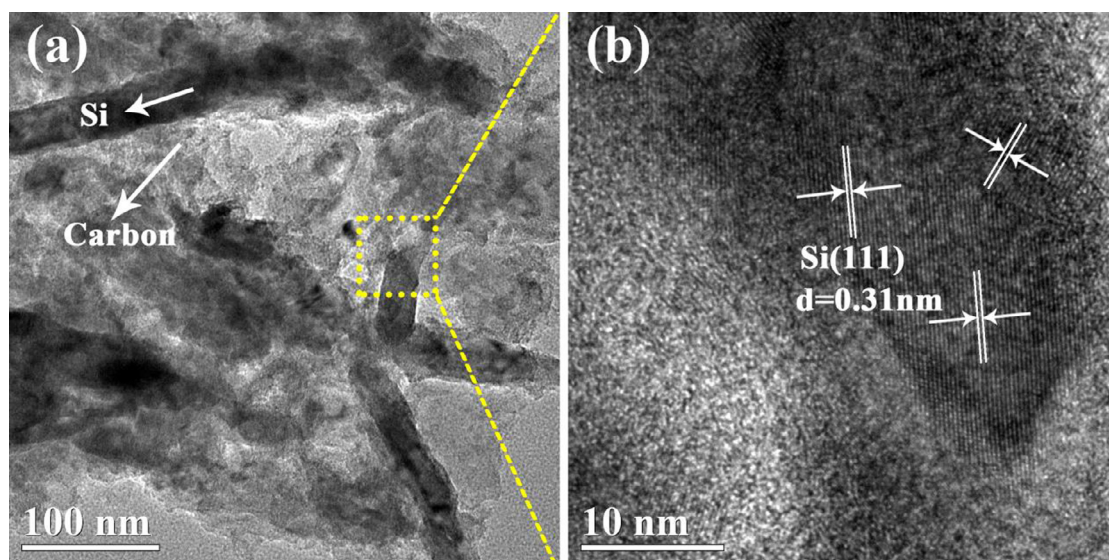


Fig. 7. TEM images of Si/C@NGs composite (a) and the HRTEM image of Si/C@NGs composite (b).

5th, 25th, 50th and 100th cycle. In the first cycle, the discharge capacity of Si/C@NGs composite electrode is $556.0 \text{ mA h g}^{-1}$ ($2644.8 \text{ mA h g}^{-1}$ vs. Si) with a Coulombic efficiency of 82.8%.

The irreversible capacity loss of Si/C@NGs in the first cycle is due to the formation of SEI layer on the electrode surface between 0.6 V and 0.9 V [32].

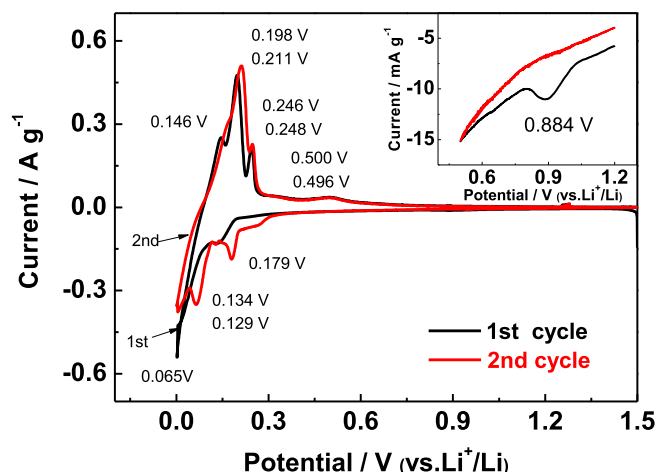


Fig. 8. Cyclic voltammetry curves of Si/C@NGs electrode from 1.5 V to 0.001 V at a scan rate of 0.05 mV s^{-1} .

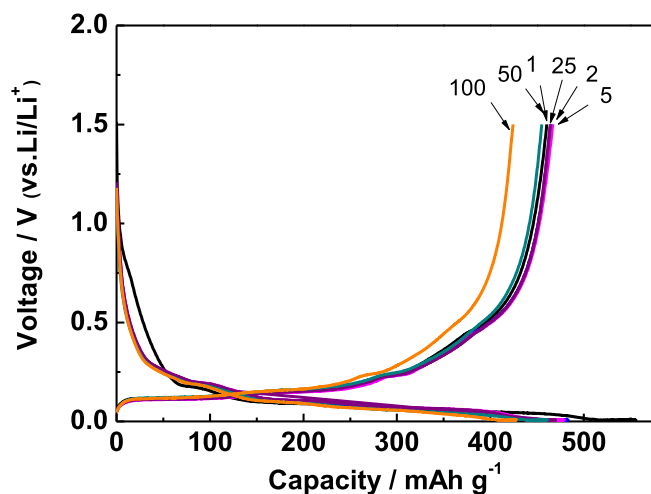


Fig. 9. The discharge/charge curves of Si/C@NGs in the 1st, 2nd, 5th, 25th, 50th and 100th cycle between 0.01 and 1.5 V at a current density of 0.1 A g^{-1} .

Fig. 10 illustrates the cycling performance of Si, NG and Si/C@NGs composite electrode, and the Coulombic efficiency vs. cycle number of Si/C@NGs composite electrode. The Coulombic efficiency increased to 96.3% at the second cycle and was even 99.1% after 100 cycles. The discharge capacity of Si/C@NGs composite electrode are $483.3 \text{ mA h g}^{-1}$ ($2073.6 \text{ mA h g}^{-1}$ vs. Si) in the second cycle, $461.7 \text{ mA h g}^{-1}$ ($1855.6 \text{ mA h g}^{-1}$ vs. Si) after 50 cycles, and remained $428.1 \text{ mA h g}^{-1}$ ($1524.0 \text{ mA h g}^{-1}$ vs. Si) after 100 cycles, which is higher than that of Si (69.9 mA h g^{-1}) and NG electrode ($349.4 \text{ mA h g}^{-1}$). Compared with the study that initial columbic efficiency of micro-sized Si particle mixed with PAN was 66.7% and the capacity remained around 900 mA h g^{-1} at 0.2 C after 120 cycles.[33] Si/C@NGs composite has higher first cycle efficiency and better cycling stability. The better cycling stability of Si/C@NGs than pure Si and higher capacity than NG electrode could be attributed to the reasonable loading of Si (6.7 wt%) and rational structural design by applying SAN and graphite backbones. And Fig. S6 shows the Nyquist plots of Si, NG and Si/C@NGs after the 3th cycle, discharged to 1.5 V in an open-circuit potential. The Si/C@NGs anode exhibited a smaller charge-transfer resistance than Si anode, indicating faster charge transfer kinetics of the Si/C@NGs than Si anode.

To identify the change of Si/C@NGs electrode thickness before and after 30 cycles, cross-sectional SEM images were shown in Fig. 11. The Si/C@NGs electrode reveals 12.7% increase in thickness after 30 cycles without obvious inter-particle cleavage, electrical contact loss or capacity fading.

Fig. 12a reveals the rate performance of Si, NG particles and Si/C@NGs composite at different current densities from 0.1 to 1.0 A g^{-1} . At the lower current density of 0.2, 0.3 and 0.4 A g^{-1} , the discharge capacity of Si/C@NGs are 420.6, 389.2 and $357.1 \text{ mA h g}^{-1}$, which are higher than that of Si (197.9 , 70.4 and 2.3 mA h g^{-1}) and NG (339.2 , 309.3 and $275.0 \text{ mA h g}^{-1}$). With the increase of current density to 0.5 A g^{-1} , the discharge capacity of Si/C@NGs ($315.2 \text{ mA h g}^{-1}$) is much higher than Si (1.2 mA h g^{-1}). Si/C@NGs composite also delivers higher discharge capacity of 203.5 and $137.5 \text{ mA h g}^{-1}$ than Si and NG even at 0.8 and 1.0 A g^{-1} . As shown in Fig. 12b, the discharge capacity of calculated pure Si (contribution from Si/C@NGs Si/C@NGs) decreases from 2705.4 to $937.4 \text{ mA h g}^{-1}$ when current density increases from 0.1 to 1.0 A g^{-1} , while Si drops sharply from 2450.3 to 1.8 mA h g^{-1} , indicating better rate performance of calculated pure

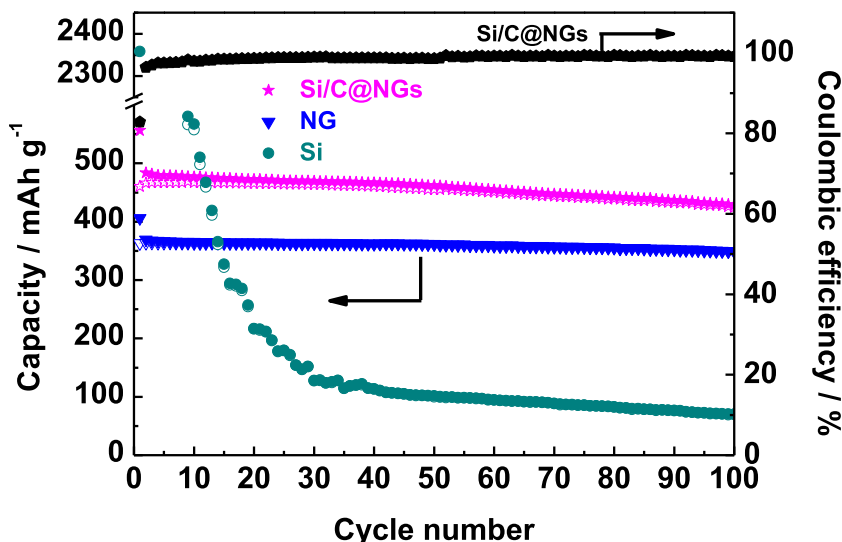


Fig. 10. The cycling performance of Si/C@NGs, NG and Si for 100 cycles between 0.01 and 1.5 V at a current density of 0.1 A g^{-1} .

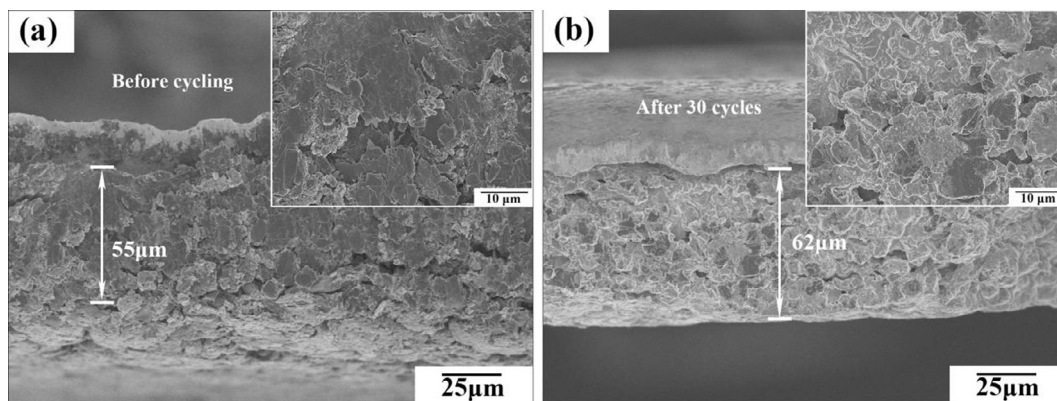


Fig. 11. Cross-sectional view of Si/C@NGs electrodes before cycling (a) and after 30 cycles (b).

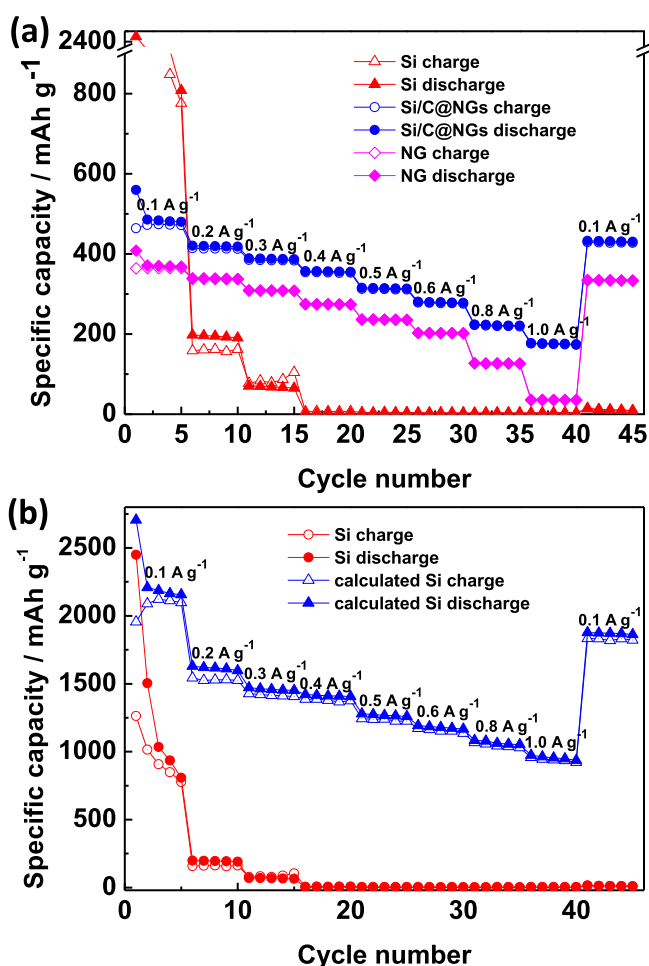


Fig. 12. Rate capacity of Si, NG and Si/C@NGs (a), and Si and calculated pure Si contribution from Si/C@NGs (b) in the potential window between 0.01 V and 1.5 V.

Si than Si. The excellent rate capability of Si/C@NGs composite may be attributed to rational structural with twice of amorphous carbon coating of sub-micron Si plates, which further ensures the expansion of Si through voids space inside the coating, while maintaining its electrical conductivity and continuity as well.

4. Conclusions

The irregularly flake-shaped sub-micron silicon modified with SA was successfully encapsulated in SAN matrix by dispersion

polymerization. The surface hydrophobic treatment of Si is of significant importance to achieve homogeneous polymer coating. The Si/C@NGs was prepared by spray-drying and pyrolysis process assisted self-assembly of Si/SAN and NG. The Si/C@NGs composite anode exhibited a high initial efficiency of 82.8% and stable cycling performance with the initial discharge capacity of 556 mA h g⁻¹ and capacity of 428.1 mA h g⁻¹ after 100 cycles at a constant current density of 0.1 A g⁻¹. The Si/C@NGs has the following advantages when used for Li-ion anodes: 1) low cost, sub-micrometer size Si nanoplates prepared by ball-milling of bulk Si can be effectively used; 2) <10 wt% Si can bring a capacity improvement of 30.4% without significant reduction of the first cycle efficiency; 3) the Si/C@NG micrometer-size secondary particles has smaller surface area (9 m² g⁻¹), giving a higher volumetric energy density. Consequently, the novel Si/C@NGs self-assembly composite electrode is promising for industrial applications.

Acknowledgements

The research was financially supported by Primary Research & Development Plan of Jiangsu Province (Grant No. BE2016183), National Natural Science Foundation of China (Grant No. 51502135), Natural Science Foundation of Jiangsu Province for Youth (Grant No. BK20160960) and Postgraduate Innovation Foundation of Jiangsu Province (Grant No. KYZZ16_0242).

Appendix A. Supplementary data

Supplementary data associated with this article can be found, in the online version, at <http://dx.doi.org/10.1016/j.cej.2016.12.072>.

References

- [1] H. Fei, X. Liu, Z. Li, Hollow cobalt coordination polymer microspheres: a promising anode material for lithium-ion batteries with high performance, *Chem. Eng. J.* 281 (2015) 453–458.
- [2] Y. Sun, J. Lopez, H.W. Lee, N. Liu, G. Zheng, C.L. Wu, J. Sun, W. Liu, J.W. Chung, Z. Bao, Y. Cui, A stretchable graphitic carbon/Si anode enabled by conformal coating of a self-healing elastic polymer, *Adv. Mater.* 28 (2016) 2455–2461.
- [3] J.X. Wu, X.Y. Qin, H.R. Zhang, Y.B. He, B.H. Li, L. Ke, W. Lv, H.D. Du, Q.H. Yang, F. Y. Kang, Multilayered silicon embedded porous carbon/graphene hybrid film as a high performance anode, *Carbon* 84 (2015) 434–443.
- [4] R. Xu, S. Wu, Y. Du, Z. Zhang, A facile route to dually protected Ge@GeO₂ composites as anode materials for lithium ion battery, *Chem. Eng. J.* 296 (2016) 349–355.
- [5] Y.H. Huang, C.T. Chang, Q. Bao, J.G. Duh, Y.L. Chueh, Heading towards novel superior silicon-based lithium-ion batteries: ultrasmall nanoclusters top-down dispersed over synthetic graphite flakes as binary hybrid anodes, *J. Mater. Chem. A* 3 (2015) 16998–17007.
- [6] M.T. McDowell, S.W. Lee, W.D. Nix, Y. Cui, 25th anniversary article: understanding the lithiation of silicon and other alloying anodes for lithium-ion batteries, *Adv. Mater.* 25 (2013) 4966–4985.

- [7] H. Wu, Y. Cui, Designing nanostructured Si anodes for high energy lithium ion batteries, *Nano Today* 7 (2012) 414–429.
- [8] D.C. Lin, Z.D. Lu, P.C. Hsu, H.R. Lee, N. Liu, J. Zhao, H.T. Wang, C. Liu, Y. Cui, A high tap density secondary silicon particle anode fabricated by scalable mechanical pressing for lithium-ion batteries, *Energy Environ. Sci.* 8 (2015) 2371–2376.
- [9] M. Li, X.H. Hou, Y.J. Sha, J. Wang, S.J. Hu, X. Liu, Z.P. Shao, Facile spray-drying/pyrolysis synthesis of core-shell structure graphite/silicon-porous carbon composite as a superior anode for Li-ion batteries, *J. Power Sources* 248 (2014) 721–728.
- [10] W.J. Wu, Y.H. Liang, H.Y. Ma, Y. Peng, H.B. Yang, Insights into the conversion behavior of SiO-C hybrid with pre-treated graphite as anodes for Li-ion batteries, *Electrochim. Acta* 187 (2016) 473–479.
- [11] Q. Cheng, T. Yang, Y. Li, M. Li, C.K. Chan, Oxidation-reduction assisted exfoliation of LiCoO₂ into nanosheets and reassembly into functional Li-ion battery cathodes, *J. Mater. Chem. A* 4 (2016) 6902–6910.
- [12] E.J. Shin, S. Kim, J.K. Noh, D. Byun, K.Y. Chung, H.S. Kim, B.W. Cho, A green recycling process designed for LiFePO₄ cathode materials for Li-ion batteries, *J. Mater. Chem. A* 3 (2015) 11493–11502.
- [13] N. Liu, Z.D. Lu, J. Zhao, M.T. McDowell, H.W. Lee, W.T. Zhao, Y. Cui, A pomegranate-inspired nanoscale design for large-volume-change lithium battery anodes, *Nat. Nanotechnol.* 9 (2014) 187–192.
- [14] Y.Y. Huang, D. Han, Y.B. He, Q.B. Yun, M. Liu, X.Y. Qin, B.H. Li, F.Y. Kang, Si nanoparticles intercalated into interlayers of slightly exfoliated graphite filled by carbon as anode with high volumetric capacity for lithium-ion battery, *Electrochim. Acta* 184 (2015) 364–370.
- [15] Z.L. Zhang, Y.H. Wang, W.F. Ren, Q.Q. Tan, Y.F. Chen, H. Li, Z.Y. Zhong, F.B. Su, Scalable synthesis of interconnected porous silicon/carbon composites by the Rochow reaction as high-performance anodes of lithium ion batteries, *Angew. Chem. Int. Ed.* 53 (2014) 5165–5169.
- [16] H.X. Zhang, S.L. Jing, Y.J. Hu, H. Jiang, C.Z. Li, A flexible freestanding Si/rGO hybrid film anode for stable Li-ion batteries, *J. Power Sources* 307 (2016) 214–219.
- [17] T.D. Bogart, D. Oka, X.T. Lu, M. Gu, C.M. Wang, B.A. Korgel, Lithium ion battery performance of silicon nanowires with carbon skin, *ACS Nano* 8 (2014) 915–922.
- [18] P. Wu, H. Wang, Y.M. Tang, Y. Zhou, T.H. Lu, Three-dimensional interconnected network of graphene-wrapped porous silicon spheres: in situ magnesiothermic-reduction synthesis and enhanced lithium-storage capabilities, *ACS Appl. Mater. Interfaces* 6 (2014) 3546–3552.
- [19] F.D. Liu, Z.L. Wang, Y.J. Zhou, X. Liu, Preparation of hybrid composite microspheres containing nanosilicon via micro-suspension polymerization, *J. Appl. Polym. Sci.* 133 (2016) 43101.
- [20] Y.S. Hu, R. Demir-Cakan, M.M. Titirici, J.O. Muller, R. Schlögl, M. Antonietti, J. Maier, Superior storage performance of a Si@SiO_x/C nanocomposite as anode material for lithium-ion batteries, *Angew. Chem. Int. Ed.* 47 (2008) 1645–1649.
- [21] F. Zhang, X. Yang, Y.Q. Xie, N.B. Yi, Y. Huang, Y.S. Chen, Pyrolytic carbon-coated Si nanoparticles on elastic graphene framework as anode materials for high-performance lithium-ion batteries, *Carbon* 82 (2015) 161–167.
- [22] L. Wang, B. Gao, C.J. Peng, X. Peng, J.J. Fu, P.K. Chu, K.F. Huo, Bamboo leaf derived ultrafine Si nanoparticles and Si/C nanocomposites for high-performance Li-ion battery anodes, *Nanoscale* 7 (2015) 13840–13847.
- [23] H. Wu, G.Y. Zheng, N. Liu, T.J. Carney, Y. Yang, Y. Cui, Engineering empty space between Si nanoparticles for lithium-ion battery anodes, *Nano Lett.* 12 (2012) 904–909.
- [24] X.X. Liu, D.L. Chao, Q. Zhang, H. Liu, H.L. Hu, J.P. Zhao, Y. Li, Y.Z. Huang, J.Y. Lin, Z.X. Shen, The roles of lithium-philic giant nitrogen-doped graphene in protecting micron-sized silicon anode from fading, *Sci. Rep.* 5 (2015) 15665.
- [25] Z.D. Lu, N. Liu, H.W. Lee, J. Zhao, W.Y. Li, Y.Z. Li, Y. Cui, Nonfilling carbon coating of porous silicon micrometer-sized particles for high-performance lithium battery anodes, *ACS Nano* 9 (2015) 2540–2547.
- [26] M. Chen, Z.L. Wang, A.N. Wang, W.S. Li, X. Liu, L.J. Fu, W. Huang, Novel self-assembled natural graphite based composite anodes with improved kinetic properties in lithium-ion batteries, *J. Mater. Chem. A* 4 (2016) 9865–9872.
- [27] M.S. Wang, L.Z. Fan, Silicon/carbon nanocomposite pyrolyzed from phenolic resin as anode materials for lithium-ion batteries, *J. Power Sources* 244 (2013) 570–574.
- [28] L. Gan, H.J. Guo, Z.X. Wang, X.H. Li, W.J. Peng, J.X. Wang, S.L. Huang, M.R. Su, A facile synthesis of graphite/silicon/graphene spherical composite anode for lithium-ion batteries, *Electrochim. Acta* 104 (2013) 117–123.
- [29] Y. Zhang, Y.Z. Jiang, Y.D. Li, B.B. Li, Z.H. Li, C.M. Niu, Preparation of nanographite sheets supported Si nanoparticles by in situ reduction of fumed SiO₂ with magnesium for lithium ion battery, *J. Power Sources* 281 (2015) 425–431.
- [30] H.C. Tao, M. Huang, L.Z. Fan, X.H. Qu, Effect of nitrogen on the electrochemical performance of core-shell structured Si/C nanocomposites as anode materials for Li-ion batteries, *Electrochim. Acta* 89 (2013) 394–399.
- [31] B. Fuchsbichler, C. Stangl, H. Kren, F. Uhlig, S. Koller, High capacity graphite-silicon composite anode material for lithium-ion batteries, *J. Power Sources* 196 (2011) 2889–2892.
- [32] L.G. Xue, G.J. Xu, Y. Li, S.L. Li, K. Fu, Q. Shi, X.W. Zhang, Carbon-coated Si nanoparticles dispersed in carbon nanotube networks as anode material for lithium-ion batteries, *ACS Appl. Mater. Interfaces* 5 (2013) 21–25.
- [33] C.Q. Zhang, F. Yang, D.L. Zhang, X. Zhang, C.L. Xue, Y.H. Zuo, C.B. Li, B.W. Cheng, Q.M. Wang, A binder-free Si-based anode for Li-ion batteries, *RSC Adv.* 5 (2015) 15940–15943.